# Comparing True Countercurrent and Simulated Moving-Bed Chromatographic Reactors

**Florian Lode, Marco Mazzotti, and Massimo Morbidelli**
ETH Swiss Federal Institute of Technology Zurich, Laboratorium für Technische Chemie, CH-8093 Zürich, Switzerland

*Simulated Moving Bed reactors (SMBR) combine chemical reaction and adsorptive separation within one single continuous and countercurrent unit. This integration promises substantial improvements in process performance, especially when applied to equilibrium-limited reactions involving such heat-sensitive products as fine chemicals and pharmaceuticals. In this work, the interplay among the relevant process design parameters (dimensionless ratios of the fluid and solid flow rates, and the Damköhler numbers for each section of the unit) is investigated. For this, an analytical solution of differential mass-balance equations for the corresponding true countercurrent process (TCC), using as a model system the reaction $A \rightleftharpoons B + C$ with each species exhibiting linear adsorption behavior, was developed. Based on this solution, criteria were derived for the optimum process design with respect to productivity and solvent consumption. Comparing these results with numerical simulations of an SMBR unit shows that the TCC model does not apply to SMBR units with a finite number of columns per section, that is, units of practical relevance, because the two units exhibit different residence time distributions and, hence, lead to different degrees of conversion.*

## Introduction

Reactive simulated-moving-bed processes (SMBR) are hybrid operations combining chemical reaction and adsorptive separation within one single apparatus. This process integration allows for improvements in terms of chemical conversion in the case of equilibrium limited reactions. Here, the separation of the reaction products immediately after their formation effectively suppresses the backward reaction, and complete conversion of the limiting reactant can be achieved upon one single pass through the reactor. SMB reactors thus represent an alternative to the industrially more established reactive distillation processes in applications requiring benign operating conditions, as is often the case for fine chemicals or pharmaceuticals.

A typical configuration of a reactive SMB process is shown in Figure 1 for the case of a monomolecular reaction, $A \rightleftharpoons B + C$, taking place in an inert solvent, $S$. Here, a total of eight fixed beds is interconnected in order to form a closed-loop assembly, and the inlet and outlet streams are delivered to the unit in such a way that the unit appears to be divided in four different sections comprising two columns each. The countercurrent movement of the solid phase is simulated by periodically shifting the inlet and outlet ports by one column length into the direction of the liquid flow.

As the reactant is fed to the unit in between sections 2 and 3, chemical reaction is triggered and the product species are formed. The product species with the lower affinity to the solid phase $C$ is less retained and transported by the fluid flow toward the raffinate outlet, while the more retained product $B$ is strongly adsorbed and transported into sections 2 and 1 by the movement of the solid phase. If the operating conditions are properly selected, the reactant $A$ is completely consumed within sections 2 and 3, and, therefore, is absent in either outlet stream. Within section 1, the fluid flow rate is adjusted so that the strongly retained product is desorbed from the solid phase, allowing for the recycling of pure adsorbent into section 4. Within section 4, on the other hand, fluid flow rates are low enough to allow for the adsorption of the weakly retained product, and thus for the complete re-

Correspondence concerning this article should be addressed to M. Morbidelli.
Current address of M. Mazzotti: ETH Swiss Federal Institute of Technology Zurich, Institut Für Verfahrenstechnik, Sonneggstrasse 3, CH-8092 Zürich, Switzerland.

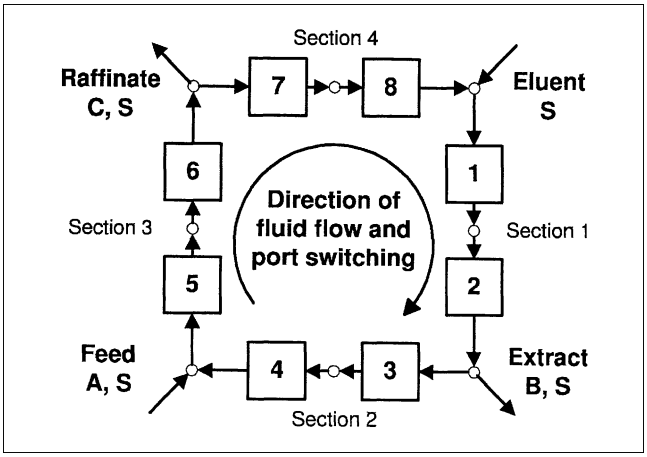


**Figure 1. Four-section SMBR.**

generation of the solvent stream before recycling to section 1.

The practical feasibility of SMB reactors has been demonstrated for a variety of chemical systems, including carbohydrate reactions (Akintoye et al., 1991; Barker et al., 1992; Hashimoto et al., 1983; Kawase et al., 2001; Shieh and Barker, 1995, 1996), the esterification of alcohols with acetic acid catalyzed by ion-exchange resins (Kawase et al., 1996; Lode et al., 2001; Mazzotti et al., 1996), and the synthesis of Bisphenol-A (Kawase et al., 1999).

As far as the design of such rather complex units is concerned, a detailed knowledge of the adsorption equilibria, as well as of the reaction kinetics involved, is necessary in order to develop a model of the SMBR process (Lode et al., 2001). Based on such a model, an optimization of the operating parameters through extensive numerical simulations is possible, in principle, although in general this procedure provides only a limited amount of insight into the interplay of the different process parameters (Duennebier et al., 2000).

In the following it is therefore intended to focus on the identification of the relevant design parameters and their effect on the unit behavior, in order to deepen the understanding of SMBR units and to define guidelines for a successful process optimization.

In the case of a nonreactive SMB process such an understanding could be obtained from an analysis of a true countercurrent chromatographic process (TCC), which can be shown to be equivalent to the SMB process provided that certain conversion rules on the operating parameters of the TCC and the SMB are fulfilled (Storti et al., 1988). In this work, a similar approach is followed for investigating the behavior of a reactive SMB process. In particular, a true countercurrent reaction process is investigated here within the framework of equilibrium theory for the case of monomolecular reactions involving species exhibiting linear adsorption equilibria. Based on an analysis of the corresponding partial differential mass balance equations, a sound framework for the description of the process behavior is devised, comprising the Damköhler numbers within the two central sections of the unit, as well as the dimensionless flow rate ratios between the fluid and the solid phase, already utilized in the case of nonreactive applications. Within such a framework, design criteria for the optimal performance of the true countercurrent reactive process in terms of solvent consumption and productivity are derived.

In order to investigate the applicability of the design criteria derived for the TCC process to the SMBR process, the performance of a reactive SMB is investigated through numerical simulations. The comparison of these results with the predictions based on the TCC model reveals substantial discrepancies, which in the case of an irreversible reaction can be explained by considering the differences in the residence-time distributions of the two reactor configurations.

## Analysis of a True Countercurrent Chromatographic Reactor

Due to the discrete movement of the inlet and outlet ports after every switch time interval, SMB units do not achieve a time-independent steady state, but rather a periodic one; that is, the unit exhibits the same time-dependent behavior during each period between two successive switches. This behavior can only be described properly by time-dependent models, necessitating the use of computation intensive numerical simulations for their solution.

In order to devise shortcut methods for the design of such units it is therefore more effective to analyze a true countercurrent reactive system (TCC), as shown in Figure 2, which indeed attains a time-independent steady state. If the four sections of the SMB are divided into a large enough number of very short subsections and the switches occur at a very high frequency to reasonably approximate the continuous countercurrent movement of the solid phase, TCC and SMB processes exhibit the same behavior given that certain geometric and kinematic equivalence rules are followed. For a process involving an adsorbent phase of porosity $\epsilon_p$ packed into columns of bed void fraction $\epsilon_b$, these rules are given by the following relationships ($j = 1, \ldots, 4$)

$$L_j = n_j L_{\text{col}}$$

$$u_s^{\text{TCC}} = \frac{(1-\epsilon_b)L_{\text{col}}}{t^*}$$

$$u_j^{\text{TCC}} = u_j^{\text{SMB}} - \frac{\epsilon_b L_{\text{col}}}{t^*}. \qquad (1)$$

Here, $L_j$ and $L_{\text{col}}$ denote the length of the $j$th section of the TCC unit and of the single column in the SMB, respectively; $n_j$ the number of columns per section in the SMB unit; $u_s^{\text{TCC}}$, $u_j^{\text{TCC}}$, and $u_s^{\text{SMB}}$ represent the superficial velocities of the solid, as well as of the fluid, phase within section $j$ for the TCC and for the SMB unit, respectively; and $t^*$ is the time period between two successive port switches in the SMB unit.

Here, a TCC model where the effects of axial dispersion and mass-transport resistance are neglected is considered. When applying this idealized model to the generic reaction $A \rightleftharpoons B + C$, with the reaction rate per unit volume given by $r = k_R f(\boldsymbol{c})$, the corresponding mass-balance equations for the

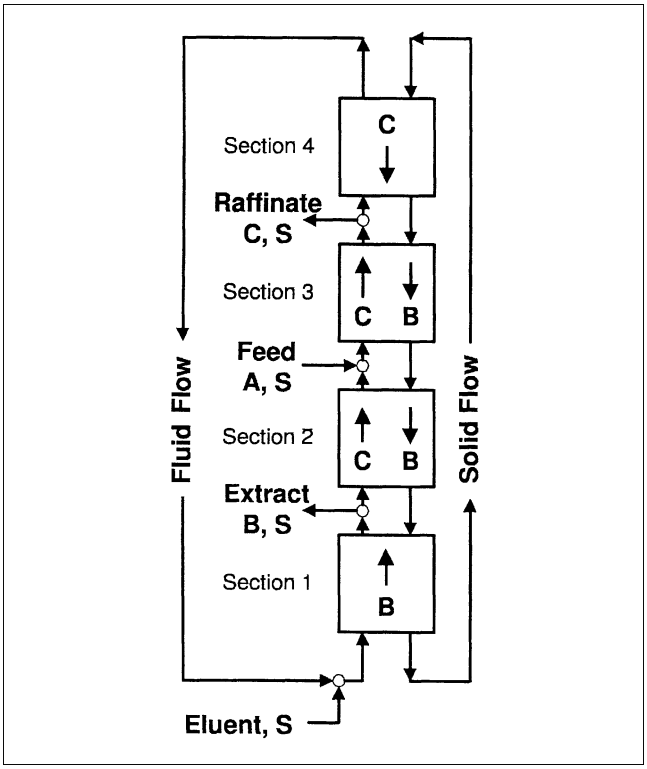


**Figure 2. Four-section TCCR.**

generic $j$th section of the TCC unit are given by

$$\frac{\partial}{\partial x_j}\left[\epsilon^* c_{i,j} + (1-\epsilon^*) q_{i,j}^{\mathrm{eq}}\right] + (1-\epsilon_p)\frac{\partial}{\partial y_j}\left[m_j c_{i,j} - q_{i,j}^{\mathrm{eq}}\right] = \nu_i Da_j f(\boldsymbol{c}_j) \quad (2)$$

$$x_j = \frac{t u_s^{\mathrm{TCC}}}{L_j}$$

$$y_j = \frac{z}{L_j}$$

$$m_j = \frac{u_j^{\mathrm{TCC}} - \epsilon_p u_s^{\mathrm{TCC}}}{(1-\epsilon_p) u_s^{\mathrm{TCC}}}$$

$$Da_j = \frac{k_R L_j}{u_s^{\mathrm{TCC}}},$$

where $x_j$ and $y_j$ are the dimensionless time and space variables; $m_j$ is the flow rate ratio parameter representing the ratio between the net fluid flow rate and the solid flow rate in the $j$th section; the Damköhler number $Da_j$ is defined as the ratio between the residence time of the solid phase in the generic section and the characteristic time for the reaction; the overall bed void fraction $\epsilon^*$ is given by $\epsilon^* = \epsilon_b + (1-\epsilon_b)\epsilon_p$; and $\nu_i$ is the stoichiometric coefficient of the $i$th species, that is, $-\nu_A = \nu_B = \nu_C = 1$.

The adsorbed phase concentrations $q_i^{\mathrm{eq}}$ are here linked to the concentrations in the fluid phase $c_i$ by a linear adsorption isotherm

$$q_i^{\mathrm{eq}} = H_i c_i, \quad (3)$$

with the reactant $A$ exhibiting an intermediate affinity toward the solid phase as compared to the reaction products, that is

$$H_B > H_A > H_C \quad (4)$$

Boundary and initial conditions for each section of the unit define the initial state of the section, as well as the compositions of the two incoming streams

$$\begin{aligned} c_{i,j} &= c_{i,j}^{\mathrm{I}}, \quad 0 \le y_j \le 1, \quad x_j = 0 \\ c_{i,j} &= c_{i,j}^{a}, \quad y_j = 0, \quad x_j \ge 0 \\ q_{i,j} &= q_{i,j}^{b}, \quad y_j = 1, \quad x_j \ge 0. \end{aligned} \quad (5)$$

In the absence of chemical reaction, that is, for the purely separative case, it has been shown that, as far as steady-state operation is concerned, the separation performance of the unit is determined only by the value of the flow rate ratio parameter, $m_j$, within each section of the unit (Storti et al., 1988). The same framework provides an adequate basis for also discussing the reactive process, but the presence of chemical reaction necessitates that additional parameters, such as the Damköhler numbers appearing in Eq. 2, are accounted for.

In the following the interplay of the flow rate ratios and the Damköhler numbers is investigated in detail for both an irreversible reaction $A \rightarrow B + C$, as well as a reversible one, $A \rightleftharpoons B + C$. The goal is to design the process parameters in a way to obtain complete separation of the reaction products $B$ and $C$, as well as a specified degree of conversion of the reactant $A$.

For this, an analytical solution for the steady-state behavior of a four-section reactive TCC unit is investigated (Figure 2). Here, the solid is transported from the top through all four sections at a constant velocity $u_s^{\mathrm{TCC}}$ before being recycled from section 1 to section 4. The liquid phase enters the unit from the bottom at the velocity $u_1^{\mathrm{TCC}}$. In between sections 1 and 2 the strongly retained product $B$ is withdrawn through the extract stream while the reactant $A$ is fed at a concentration of $c_A^F$ between sections 2 and 3, and the weakly adsorbed product $C$ is collected in the raffinate stream between sections 3 and 4. Finally, the liquid leaving section 4 is mixed with a makeup stream of pure solvent and recycled to section 1.

In the absence of mass-transfer limitations, the solid and the fluid phases within each section are at equilibrium at any time and spatial location. It can then be shown that there has to be at least one discontinuity in the species concentrations at either the inlet or outlet boundary of each section, given that the solid and the liquid phases passing each other at each section end are not necessarily at equilibrium. Note, however, that this is not a propagating shock transition like

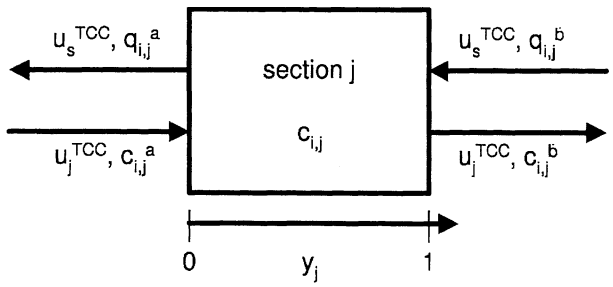


**Figure 3. Standard section of a true countercurrent unit.**

those occurring in nonlinear chromatography, but that this concentration jump remains located at the boundaries only, that is, it is a so-called boundary discontinuity. The liquid and solid phase concentrations just outside each section are linked to the concentrations inside the unit by one mass-balance equation for each component at each section end (see Figures 2 and 3 for the notation)

$$\left(m_j + \frac{\epsilon_p}{1-\epsilon_p}\right) c_{i,j}^a - \left(1 + \frac{\epsilon_p}{(1-\epsilon_p)H_i}\right) q_{i,j}^a = (m_j - H_i)\, c_{i,j}(0^+) = (m_j - H_i)\, c_{i,j}^0 \quad (6)$$

$$\left(m_j + \frac{\epsilon_p}{1-\epsilon_p}\right) c_{i,j}^b - \left(1 + \frac{\epsilon_p}{(1-\epsilon_p)H_i}\right) q_{i,j}^b = (m_j - H_i)\, c_{i,j}(1^-) = (m_j - H_i)\, c_{i,j}^1. \quad (7)$$

Within each section, the concentration profiles are continuous and given by the partial differential equations just described (Eq. 2).

In order to find a solution to the system of partial differential equations the method of characteristics is applied here. Substituting the adsorption isotherm (Eq. 3) into the differential mass-balance equation for each species (Eq. 2) yields

$$\left[\epsilon^* + (1-\epsilon^*)H_i\right] \frac{\partial c_{i,j}}{\partial x_j} + (1-\epsilon_p)(m_j - H_i) \frac{\partial c_{i,j}}{\partial y_j} = \nu_i Da_j f(\underline{c}_j). \quad (8)$$

The corresponding characteristic equations are constituted by the following system of ordinary differential equations

$$\frac{dx_j}{ds} = \epsilon^* + (1-\epsilon^*)H_i \quad (9)$$

$$\frac{dy_j}{ds} = (1-\epsilon_p)(m_j - H_i) \quad (10)$$

$$\frac{dc_{i,j}}{ds} = \nu_i Da_j f(\underline{c}_j), \quad (11)$$

where $s$ is the coordinate along the characteristic.

By dividing Eqs. 9 and 10, it is seen that, within the physical plane $(x_j, y_j)$, the characteristic curves are parallel straight lines with slope

$$\frac{dx_j}{dy_j} = \frac{\epsilon^* + (1-\epsilon^*)H_i}{(1-\epsilon_p)(m_j - H_i)} = \sigma_{i,j}. \quad (12)$$

Note in particular that the slope of the characteristic $\sigma_{i,j}$ is independent of the species concentration and of the reaction rate, and that its sign depends only on the difference between the flow rate ratio $m_j$ and the Henry coefficient of each species. The concentration of each species, though, varies along the characteristics according to Eq. 11, where in general the function $f(\underline{c}_j)$ couples the equations for the different species.

Since a different characteristic with slope $\sigma_{i,j}$ is defined for each species $i$, it would be difficult to integrate Eq. 11 for $i = A, B, C$ at the same time. This difficulty can be overcome by dividing Eqs. 10 and 11 term by term in order to express the concentrations of all species in terms of the same independent variable $y_j$, that is, the dimensionless space coordinate within the $j$th section

$$\frac{dc_{A,j}}{dy_j} = -\frac{Da_j f(\underline{c}_j)}{(1-\epsilon_p)(m_j - H_A)} \quad (13)$$

$$\frac{dc_{B,j}}{dy_j} = \frac{Da_j f(\underline{c}_j)}{(1-\epsilon_p)(m_j - H_B)} \quad (14)$$

$$\frac{dc_{C,j}}{dy_j} = \frac{Da_j f(\underline{c}_j)}{(1-\epsilon_p)(m_j - H_C)} \quad (15)$$

The boundary conditions required for the integration of Eqs. 13 to 15 need to be derived from an analysis of the slopes of the characteristics. In particular, the sign of $\sigma_{i,j}$ defines the direction within the single TCC section in which information is propagated, and, accordingly, the location of the boundary discontinuity. In the case of the characteristics exhibiting positive slopes, that is, $\sigma_{i,j} > 0$, the information given by the boundary condition on the left end of the section $c_{i,j}^a$ is propagated into the domain of interest, hence, $c_{i,j}^0 = c_{i,j}^a$, and accordingly a boundary discontinuity occurs at the right end of the section, that is, $c_{i,j}^1 \neq c_{i,j}^b$. The reverse situation is obtained for $\sigma_{i,j} < 0$, where the situation inside the section is determined by the boundary condition at $y_j = 1$, hence, $c_{i,j}^1 = q_{i,j}^b / H_i$, and the boundary discontinuity is located at the left end of the section, that is, $q_{i,j}^a \neq H_i c_{i,j}^0$.

In the case of the process under consideration here, the sign of $\sigma_{i,j}$ for each species within one section of the unit is determined only by the difference between the flow rate ratio $m_j$ and the species' Henry coefficient $H_i$. Based on this information, only it is possible to derive criteria on the flow rate ratios within the different sections of the unit to fulfill the process specifications. As mentioned earlier, the goal of the process is to achieve a complete separation of the product species, with the more retained product $B$ being collected in the extract stream, and the less retained one $C$ being withdrawn with the raffinate, and to reach a specified conversion degree of the reactant $A$.

The necessary condition for the separation of the two products is that the more retained product $B$, and the less

retained one $C$, are absent from the solid and from the fluid recycle, respectively. Focusing first on section 1, this implies the complete desorption of the more retained product, hence, that $q^a_{B,1} = 0$. With the desorbent stream being devoid of any reacting species $c^D_i = c^a_{i,1} = 0$, the complete regeneration can be achieved only when the boundary condition at $y_1 = 0$ propagates into section 1. Accordingly, a positive value of $\sigma_{B,1}$ is required, which is equivalent to the flow rate ratio in section 1 being larger than the Henry coefficient of species $B$, that is, $m_1 > H_B$. It follows from Eq. 4 that the slope of the characteristics of species $A$ and $C$ at $y_1 = 0$ are also positive, that is, $\sigma_{C,1} > \sigma_{A,1} > 0$, and that the concentrations of all three species at the fluid inlet of section 1 are equal to zero, that is, $c^0_{i,1} = 0$. Flow rate ratios within section 1 higher than the Henry coefficient of the most adsorbable species therefore lead to a complete regeneration of the solid phase within section 1, as required.

Concerning section 4, the adsorption of the least retained component is required, which implies the condition $c^b_{C,4} = 0$. Given that the solid stream being recycled from section 1 does not comprise species $C$, that is, $q^b_{C,4} = 0$, it follows that $c^1_{C,4} = 0$, according to Eq. 7. This implies the absence of a boundary discontinuity and accordingly that $\sigma_{C,4} < 0$, or in other terms that $m_4 < H_C$. Because of Eq. 4, this condition guarantees that $\sigma_{A,4}$ and $\sigma_{B,4}$ are also negative, and thus that the fluid stream is completely regenerated within section 4.

Following a similar line of arguments, it is possible to develop criteria on the flow rate ratios within sections 2 and 3, leading to a complete separation of the reaction products, that is, $B$ and $C$. Here, in order to prevent the less retained product $C$ from reaching the extract outlet, the values of the flow rate ratios must be lower bounded by the product's Henry coefficient, that is, $m_3 > m_2 > H_C$. On the other hand, for product $B$, a negative slope of the characteristics is required in sections 2 and 3, which is equivalent to $m_2 < m_3 < H_B$.

Summarizing, the flow rate ratios within the four sections have to fulfill the following constraints in order to lead to a complete separation of the two product species, $B$ and $C$

$$m_1 > H_B \tag{16}$$

$$H_B > m_3 > m_2 > H_C \tag{17}$$

$$H_C > m_4. \tag{18}$$

As stated earlier, the conditions imposed onto sections 1 and 4 guarantee the absence of the reactant $A$ within these two sections. Focusing on central sections 2 and 3, though, and keeping in mind that $H_B > H_A > H_C$, three different cases can, as far as reactant $A$ is concerned, be distinguished as follows:

- $m_3 > m_2 > H_A$. Here, the slope of the characteristics for $A$ are positive in both central sections of the unit, and the concentration of $A$ in the entering fluid stream controls its behavior in each section, that is

$$c^0_{A,j} = c^a_{A,j}, \quad j = 2, 3. \tag{19}$$

On the other hand, the solid phase entering each of the two central sections experiences a discontinuous jump from $q^b_{A,j}$ to $q^1_{A,j}$.

- $H_A > m_3 > m_2$. This case represents exactly the opposite situation with respect to the previous case. Since the slopes of the characteristics are negative for $A$, it is always the incoming solid stream that determines its concentration profiles, leading to

$$c^1_{A,j} = \frac{q^b_{A,j}}{H_A}, \quad j = 2, 3. \tag{20}$$

In this case, the boundary discontinuity is located at $y_j = 0$, leading to $c^0_{A,j} \neq c^a_{A,j}$.

- $m_3 > H_A > m_2$. Here the slope of the characteristics is negative for section 2, but positive for section 3, so that the feed zone between sections 2 and 3 controls the behavior of both sections. The corresponding inlet conditions are given by

$$c^1_{A,2} = \frac{q^b_{A,2}}{H_A},$$

$$c^0_{A,3} = c^a_{A,3}, \tag{21}$$

with the boundary discontinuities located at $y_2 = 0$ and at $y_3 = 1$.

The resulting subdivision of the region of complete product separation within the $(m_2, m_3)$-parameter plane is illustrated in Figure 4.

Having identified one boundary condition for each species within each section, the behavior of the TCC unit can be studied by calculating the internal concentration profiles by integrating Eqs. 13 to 15 for the relevant reaction-rate expressions. In the following, an irreversible and a reversible reaction are considered separately.

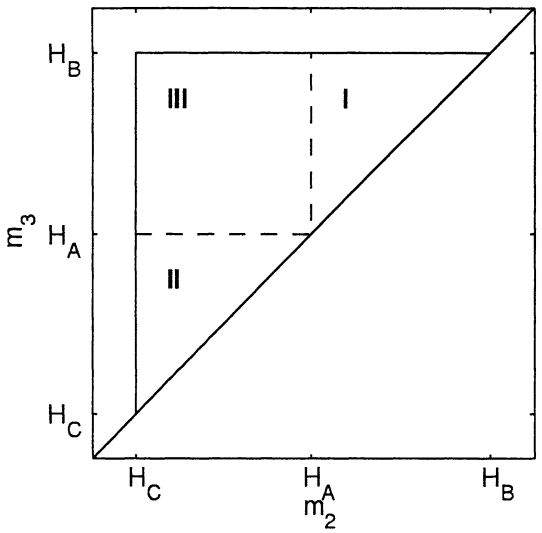


**Figure 4. Complete separation triangle and subregions identifying the locus of chemical reaction in SMBR for first-order reaction kinetics and linear sorption isotherms.**

Chemical reaction is taking place only in section 3 (I), only in section 2 (II), or in both of sections 2 and 3 (III).

### *Irreversible reaction, $A \rightarrow B + C$*

In the case of a linear irreversible reaction $f(\mathbf{c}) = c_A$ and the steady-state ODE for species $A$ (Eq. 13) is independent of the concentrations of $B$ and $C$. It can be directly solved for the concentration profiles of $A$ within the two central sections. With the concentrations of $A$ known in both outlet streams, it is then straightforward to calculate the conversion of $A$ within the unit

$$X = 1 - \frac{u^E c_A^E + u^R c_A^R}{u_A^F c_A^F} = 1 - \frac{(m_1 - m_2)c_A^E + (m_3 - m_4)c_A^R}{(m_3 - m_2)c_A^F}. \quad (22)$$

Depending on the value of the flow rate ratios relative to the Henry coefficient of the reactant, three cases have to be distinguished:

- $m_3 > m_2 > H_A$. Here, the concentration of $A$ at the left end of section 2 is equal to zero, that is, $c_{A,2}^0 = 0$, and an integration of Eq. 13 shows that the reactant is absent in all of section 2. A reaction occurs only within the third section, and the corresponding concentration profile of $A$ can be obtained by enforcing the condition that the flow of $A$ through the feed inlet must be equal to its flow through the left end of section 3, thus obtaining $c_{A,3}^0$ and by integrating Eq. 13 with $j = 3$

$$c_{A,3}^0 = \frac{m_3 - m_2}{m_3 - H_A} c_A^F \quad (23)$$

$$c_{A,3} = \frac{m_3 - m_2}{m_3 - H_A} \exp\left( - \frac{Da_3 y_3}{(1 - \epsilon_p)(m_3 - H_A)} \right) c_A^F. \quad (24)$$

Using Eq. 24 with $y_3 = 1$, enforcing the condition that the amount of $A$ passing through the right end of section 3 must be the same as its amount in the raffinate stream, and substituting the result into Eq. 22, yields

$$X = 1 - \exp\left( - \frac{Da_3}{(1 - \epsilon_p)(m_3 - H_A)} \right). \quad (25)$$

Conversion is thus only determined in this case by the Damköhler number in section 3 and by the difference between $m_3$ and $H_A$.

Obviously higher Damköhler numbers or, equivalently, an increasing length of section 3 for a given system, enhances the time available for the reaction to occur, and therefore the conversion, to occur. The term in the denominator takes into account that for given $Da_3$, and hence for a given solid flow rate, the residence time of $A$ can be tuned through variations of the fluid flow rate. In particular, complete conversion is achieved for the flow rate ratio of section 3 approaching the limit of $H_A$, leading to an infinite residence time of the reactant within this section. Because section 2 is nonreactive, neither the length of this section nor the exact value of $m_2$ is of importance for the performance of the unit.

- $H_A > m_3 > m_2$. These conditions represent exactly the opposite situation with respect to the case just discussed, hence $c_{A,3} = 0$, and the following expression can be derived in a similar way

$$c_{A,2}^1 = \frac{m_3 - m_2}{H_A - m_2} c_A^F \quad (26)$$

$$c_{A,2} = \frac{m_3 - m_2}{H_A - m_2} \exp\left( \frac{Da_2(1 - y_2)}{(1 - \epsilon_p)(m_2 - H_A)} \right) c_A^F, \quad (27)$$

thus yielding

$$X = 1 - \exp\left( - \frac{Da_2}{(1 - \epsilon_p)(H_A - m_2)} \right). \quad (28)$$

The resulting expression is completely equivalent to Eq. 25.

- $m_3 > H_A > m_2$. Since in this case $\sigma_{A,2} < 0 < \sigma_{A,3}$, it follows that $c_A^F = c_{A,3}^a = q_{A,2}^b / H_A$, and that both sections are utilized for the reaction. Integrating Eq. 13 for $j = 2$ and $j = 3$ yields

$$c_{A,2} = \exp\left( - \frac{Da_2(1 - y_2)}{(1 - \epsilon_p)(H_A - m_2)} \right) c_A^F \quad (29)$$

$$c_{A,3} = \exp\left( - \frac{Da_3 y_3}{(1 - \epsilon_p)(m_3 - H_A)} \right) c_A^F, \quad (30)$$

thus leading to

$$X = 1 - \frac{H_A - m_2}{m_3 - m_2} \exp\left( - \frac{Da_2}{(1 - \epsilon_p)(H_A - m_2)} \right) - \frac{m_3 - H_A}{m_3 - m_2} \exp\left( - \frac{Da_3}{(1 - \epsilon_p)(m_3 - H_A)} \right). \quad (31)$$

Equations 25, 28, and 31 define loci of constant conversion $X$ in the operating parameter plane $(m_2, m_3)$, that is, contour lines. In particular, Eqs. 25 and 28 define a horizontal and vertical line, respectively, whereas Eq. 31 defines a curve. This is illustrated in Figure 5 for a model system where $H_A = 1.0$, $H_B = 1.5$, and $H_C = 0.5$, and Damköhler numbers are constant, namely $Da_2 = Da_3 = 1$. The curves corresponding to $X = 0.95$ (solid line), $X = 0.90$ (broken line), and $X = 0.80$ (dash-dotted line) are drawn.

It is rather clear that points in the $(m_2, m_3)$ plane belonging to the region between the solid line and the diagonal achieve a conversion equal to or larger than 95%, and similarly for each contour line $X = \text{const}$. As anticipated, contour lines are made up of one curve connecting two straight segments. The latter, when prolonged, intersect in a point belonging to the curve corresponding to the same value of $X$, as shown by the dotted lines in Figure 5.

For constant Damköhler numbers, the conversion decreases within the $(m_2, m_3)$ parameter plane as the distance between the operating point and the point given by $m_2 = m_3 = H_A$ increases, as is shown in Figure 5 for the 90% conversion case (broken line) and 80% conversion case (dash-dotted line).

It is worth noting that the results obtained for $A$ are completely independent of the adsorptive properties of the prod-

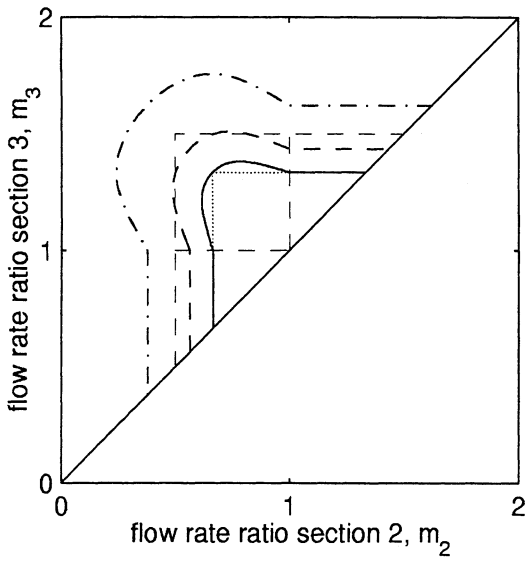


**Figure 5. Lines of 95% (solid line), 90% (dashed line), and 80% (dash-dotted line) conversion for the irreversible reaction $A \rightarrow B + C$ under conditions of constant Damköhler numbers, $Da_2 = Da_3 = 1$; Henry coefficient for the reactant, $H_A = 1$; $\epsilon_p = 0$.**

Complete separation triangle with subregions represented by thin dashed lines.

uct species $B$ and $C$. However, complete separation of the products $B$ and $C$ is guaranteed only within the complete separation region $H_C < m_2 < m_3 < H_B$ illustrated in Figure 4. This is also shown in Figure 5 for the sake of clarity. Operating points in the complete separation region achieve the conversion specified by the contour line to which they belong (for the given set of Damköhler numbers), as well as complete separation of the products. On the contrary, points outside the complete separation region, for example, those on the contour line corresponding to $X = 0.80$, achieve the specified conversion, but identify operations where the extract is contaminated with $C$, or the raffinate with $B$, or both these cases occur at the same time.

### *Implications for optimal process design*

In addition to achieving a sufficient degree of conversion and high purities of the outlet streams, the chromatographic reactor is also required to operate under economically favorable conditions. Here, the process performance is primarily determined by two parameters, namely the desorbent requirement (DR), that is, the amount of desorbent makeup consumed per mole of converted reactant, and the productivity (PR) defined as the molar amount of reactant converted per unit time and per unit reactor volume. Within the framework presented earlier, these parameters can be expressed as

Desorbent requirement:

$$DR = \frac{u^D}{u^F c_A^F X} = \frac{m_1 - m_4}{(m_3 - m_2) X c_A^F} \tag{32}$$

Productivity:

$$PR = \frac{u^F c_A^F X}{L_2 + L_3} = \frac{(m_3 - m_2) X k_R c_A^F}{Da_2 + Da_3}. \tag{33}$$

Concerning productivity, it has to be noted that in the framework of equilibrium theory the regeneration of the solid and fluid phases in sections 1 and 4 occurs instantaneously, and the required length of the section is therefore equal to zero. Therefore, the denominator in the expression defining the productivity takes into account the whole volume of the unit. However, in practical applications the efficiency of the regeneration sections is finite and the use of sections of finite dimensions is required. In these cases, the productivity of the unit is therefore lower than the values found here, but provided that the regeneration sections are well designed, the optimum design criteria derived here for the reactive part of the unit are also valid for the practical applications. For the desorbent requirement, the term in the numerator can be minimized by adjusting the flow rate ratios to the Henry coefficients of the two products $m_1 = H_B$ and $m_4 = H_C$, that is, to the lower and upper bound defined by the product separation requirement (Eq. 16).

The purity of the products in the extract and raffinate are closely related to the degree of conversion. Under the assumption that $B$ and $C$ are completely separated, that is, in the region $H_C < m_2 < m_3 < H_B$, only the unreacted $A$ can pollute the product streams. Simple overall material balances allow showing that the solvent free purities of extract and raffinate attain the following values

$$P_B^E = 1, \quad P_C^R = X \quad \text{for } m_3 > m_2 > H_A \tag{34}$$

$$P_B^E = X, \quad P_C^R = 1 \quad \text{for } H_A > m_3 > m_2 \tag{35}$$

$$P_B^E > X, \quad P_C^R > X \quad \text{for } m_3 > H_A > m_2. \tag{36}$$

With the degree of conversion being constrained by the purity specifications, the optimization problem reduces to determining at constant conversion the flow rate ratios $m_2$ and $m_3$ that optimize the $DR$ and $PR$. From Eqs. 32 and 33, for a given set of Damköhler numbers, this implies maximizing the difference between $m_3$ and $m_2$ under the constraint of constant degree of conversion.

With reference to the solid curve $X = 0.95$ in Figure 5, it can be inferred that the maximum $(m_3 - m_2)$ value is attained where the two dotted straight segments intersect, that is

$$m_2|_{\text{opt}} = H_A + \frac{Da_2}{(1 - \epsilon_p)\ln(1 - X)} \tag{37}$$

$$m_3|_{\text{opt}} = H_A - \frac{Da_3}{(1 - \epsilon_p)\ln(1 - X)}. \tag{38}$$

This is true in general, as can be proved analytically by solv-

ing the equation

$$\left.\frac{d(m_3-m_2)}{dm_2}\right|_X = \left.\frac{\partial(m_3-m_2)}{\partial(m_2)}\right|_{m_3} + \left.\frac{\partial(m_3-m_2)}{\partial(m_3)}\right|_{m_2} \frac{-\left.\frac{\partial X}{\partial m_2}\right|_{m_3}}{\left.\frac{\partial X}{\partial m_3}\right|_{m_2}} = 0: \quad (39)$$

Substituting the result into Eq. 31 yields Eqs. 37 and 38, as expected. These apply for given values of $Da_2$ and $Da_3$.

Within the complete separation region, the maximum value of $(m_3 - m_2)$ is achieved at the vertex where $m_2 = H_C$ and $m_3 = H_B$. At this point, the required conversion degree $X$ can be attained by tuning the Damköhler number; the following values are obtained from Eqs. 37 and 38

$$Da_2|_{\text{opt}} = -(H_A - H_C)(1-\epsilon_p)\ln(1-X) \quad (40)$$

$$Da_3|_{\text{opt}} = -(H_B - H_A)(1-\epsilon_p)\ln(1-X), \quad (41)$$

and allow for the achievement of the minimum desorbent requirement and the maximum productivity, namely,

$$DR|_{\text{opt}} = \frac{1}{Xc_A^F} \quad (42)$$

$$PR|_{\text{opt}} = \frac{-Xk_R c_A^F}{(1-\epsilon_p)\ln(1-X)}. \quad (43)$$

It can be readily observed that $DR$ improves for increasing conversion, whereas the opposite occurs to $PR$, which increases for less stringent purity requirements, as expected. Thus summarizing, for any required conversion degree $X$, optimal performance is achieved for $m_2 = H_C$ and $m_3 = H_B$, that is, the vertex of the complete separation region of the two products, for the Damköhler numbers given by Eqs. 37 and 38. It is worth noting that under these conditions the purity values are given by the following relationships

$$P_B^E = \frac{X(H_B - H_C)}{(H_A - H_C) + X(H_B - H_A)} \quad (44)$$

$$P_C^R = \frac{X(H_B - H_C)}{(H_B - H_A) + X(H_A - H_C)}. \quad (45)$$

### *Reversible reaction, $A \rightleftharpoons B + C$*

In the case of a reversible reaction with first-order forward reaction and second-order backward reaction, the rate expression is given by

$$f(\boldsymbol{c}) = c_A - \frac{c_B c_C}{K_{\text{eq}}}. \quad (46)$$

For the set of ODEs (Eqs. 13 to 15) governing the behavior of the TCC process in this case, the same boundary conditions as described for the irreversible reaction apply. Although the ODE system is coupled, it can be reduced to one single ODE with the reactant concentration as the dependent variable by dividing Eqs. 14 and 15 term by term by Eq. 13, thus leading to

$$\frac{dc_{B,j}}{dc_{A,j}} = -\frac{m_j - H_A}{m_j - H_B} = \beta_j \quad (47)$$

$$\frac{dc_{C,j}}{dc_{A,j}} = -\frac{m_j - H_A}{m_j - H_C} = \gamma_j. \quad (48)$$

By integrating Eqs. 47 and 48, expressions relating the variations in the concentration of the product species, $B$ and $C$, within one section to the corresponding variation in the concentration of the reactant, $A$, are obtained

$$c_{B,j} - c_{B,j}^0 = \beta_j\left(c_{A,j} - c_{A,j}^0\right) \quad (49)$$

$$c_{C,j} - c_{C,j}^0 = \gamma_j\left(c_{A,j} - c_{A,j}^0\right). \quad (50)$$

These have been obtained by integrating from left to right, but similar expressions with superscript 1 instead of 0 are obtained when integrating from right to left.

Substituting Eqs. 49 and 50 into Eq. 13, an ordinary differential equation for the concentration profile of $A$ inside section $j$ is obtained that leads to

$$\int_{c_{A,j}^0}^{c_{A,j}} \frac{dc_{A,j}}{w_{1,j}c_{A,j}^2 + w_{2,j}c_{A,j} + w_{3,j}} = -\frac{Da_j}{(1-\epsilon_p)(m_j - H_A)} y_j, \quad (51)$$

where

$$w_{1,j} = -\frac{\beta_j\gamma_j}{K_{\text{eq}}}$$

$$w_{2,j} = 1 - \frac{1}{K_{\text{eq}}}\left(\beta_j c_{C,j}^0 + \gamma_j c_{B,j}^0\right) + 2\frac{\beta_j\gamma_j}{K_{\text{eq}}}c_{A,j}^0$$

$$w_{3,j} = \frac{1}{K_{\text{eq}}}\left[-c_{B,j}^0 c_{C,j}^0 + \left(\beta_j c_{C,j}^0 + \gamma_j c_{B,j}^0\right)c_{A,j}^0 - \beta_j\gamma_j\left(c_{A,j}^0\right)^2\right].$$

Two forms of the solution have to be considered, depending on the sign of the discriminant, that is, $\Delta = 4w_{1,j}w_{3,j} - (w_{2,j})^2$

$$\frac{2}{\sqrt{\Delta}}\left(\arctan\frac{2w_{1,j}c_{A,j}^1 + w_{2,j}}{\sqrt{\Delta}} - \arctan\frac{2w_{1,j}c_{A,j}^0 + w_{2,j}}{\sqrt{\Delta}}\right) = -\frac{Da_j}{(1-\epsilon_p)(m_j - H_A)} \quad (\Delta > 0), \quad (52)$$

$$\frac{1}{\sqrt{-\Delta}}\left(\ln\frac{2w_{1,j}c^1_{A,j}+w_{2,j}-\sqrt{-\Delta}}{2w_{1,j}c^1_{A,j}+w_{2,j}+\sqrt{-\Delta}} - \ln\frac{2w_{1,j}c^0_{A,j}+w_{2,j}-\sqrt{-\Delta}}{2w_{1,j}c^0_{A,j}+w_{2,j}+\sqrt{-\Delta}}\right) = -\frac{Da_j}{(1-\epsilon_p)(m_j-H_A)} \quad (\Delta<0), \quad (53)$$

The case $\Delta = 0$ is not considered here, since it is *nongeneric*, that is, it is obtained through a very special combination of values of the physical parameters that makes little sense to insist on.

Each of these equations comprises an analytical relation between the liquid-phase concentrations of the reactant at the inlet and at the outlet of section $j$, that is, between $c^0_{A,j}$ and $c^1_{A,j}$. Since one of these two quantities is known from the boundary conditions, the remaining one has to be found by numerically solving either Eq. 52 or Eq. 53. It is worth noting that, depending on the values of the flow rate ratios and of the Damköhler numbers, both functional forms of the solution can indeed occur.

The shape of the isoconversion lines within the $(m_2,m_3)$-parameter plane shall be discussed using a model system characterized by the same adsorptive properties as in the case of the irreversible reaction described earlier, that is, $H_A = 1$, $H_B = 1.5$, $H_C = 0.5$, and $Da_2 = Da_3 = 1$.

The isoconversion curves corresponding to a conversion degree of $X = 0.90$ are drawn in Figure 6 for different values of the reaction equilibrium constant, namely $K_{eq} = 10$ (dotted line), $K_{eq} = 1.0$ (dashed line), and $K_{eq} = 0.1$ (dash-dotted line) in addition to the irreversible reaction case (solid line). Also, for the sake of clarity the complete separation triangle $H_C < m_2 < m_3 < H_B$ is reported.

It can be readily observed that the smaller the $K_{eq}$ value, the smaller the region where 90% conversion or more can be achieved with respect to the irreversible reaction. Close to the diagonal, the isoconversion lines for finite $K_{eq}$ values are very similar to the ones for the irreversible reaction case. This can be understood by considering that under very dilute conditions corresponding to $m_3 \to m_2$, that is, $u^F \to 0$, the second-order backward reaction is reduced more than the first-order forward reaction. On the other hand, in the neighborhood of the optimal point, the reversible case can achieve only a worse performance than the irreversible case for the given values of the Damköhler numbers. Compared to the irreversible reaction, the maximum productivity at 90% conversion is reduced by about 12% in the case of $K_{eq} = 10$, but by 38% and by 71% in the case of $K_{eq} = 1$ and 0.1, respectively.

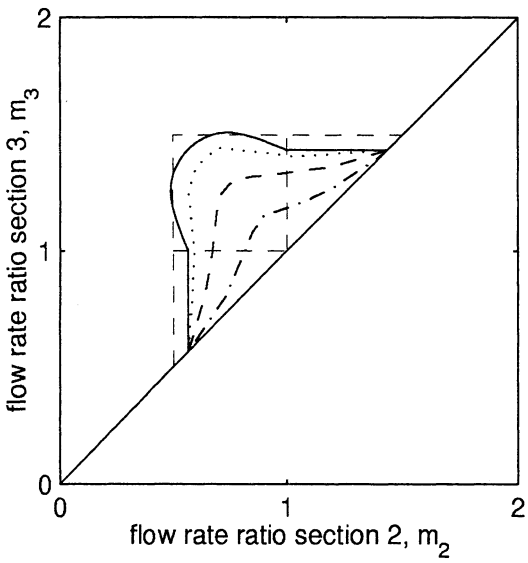


**Figure 6. Lines of 90% conversion for the reversible reaction $A \rightleftharpoons B + C$ under conditions of constant Damköhler numbers, $Da_2 = Da_3 = 1$, as compared to an irreversible reaction $A \to B + C$ (solid line); $K_{eq} = 10$ (dotted line); $K_{eq} = 1$ (dashed line); $K_{eq} = 0.1$ (dash-dotted line); Henry coefficients: $H_A = 1$; $H_B = 1.5$; $H_C = 0.5$.**

Complete separation triangle with subregions represented by thin dashed lines.

## Comparison of TCCR with SMBR

In the first part of this work, the performance of a true countercurrent reactive adsorption process characterized by linear adsorption isotherms, infinite mass-transfer kinetics, and negligible axial dispersion has been analyzed in order to achieve a deeper understanding of how operating parameters control process performance.

While the behavior of the true countercurrent process has been shown to be completely equivalent to the corresponding simulated moving-bed process for a purely separative system, this is not necessarily the case for a reactive process. In particular, the performance of a reactive unit, as compared to the purely separative one, depends upon the residence time of the reactant within the different sections of the unit. Accordingly, in the following the residence time distribution (RTD) for an SMB system with discrete shifting of the columns is compared to that of the corresponding TCC process. The results obtained from the RTD analysis are assessed by comparison with detailed numerical simulations of a simulated moving-bed reactor.

The synthesis of methyl acetate from methanol and acetic acid, catalyzed by a sulfonated ion-exchange resin, under infinite dilution conditions in methanol was chosen for these simulations. The sorption isotherms described previously can be approximated under these conditions by linear isotherms, with Henry coefficients $H_A = 0.063$, $H_W = 2.60$, and $H_E = 0.038$ for acetic acid, water, and methyl acetate, respectively (Lode et al., 2001). Furthermore, because methanol is present in large excess, the esterification reaction is of zeroth order in methanol and can be approximated by the monomolecular reaction, $A \to W + E$, where the equilibrium limitation is disregarded in order to obtain an analytical solution of the model equations. A pseudo-first-order expression for the reaction rate is adopted, which accounts for reaction in both the fluid and the solid phase

$$r = k_R c_A = \epsilon^* k_L c_A + (1-\epsilon^*) k_S H_A c_A = \epsilon^* r_L + (1-\epsilon^*) r_S \quad (54)$$

In the case of the methyl acetate synthesis catalyzed by a sulfonated ion-exchange resin the reaction rate in the liquid phase can be considered negligible, $k_L \ll k_R H_A$; hence, Eq. 54 reduces to $r = (1-\epsilon^*) r_S = (1-\epsilon^*) k_S H_A c_A$ for the model system, with the reaction rate constant in the solid phase given by $k_S = 2.42\ \text{min}^{-1}$ (Lode et al., 2001).

Due to the small value of the Henry coefficient of the reactant, among the subregions of the complete separation triangle in the $(m_2,m_3)$-plane, the one characterized by the reaction taking part predominantly in section 3, that is, region I in Figure 4, is of prime importance. Accordingly, for the sake of simplicity but without loss of generality, attention here is focused only on operating points in this region, that is, $m_3 > m_2 > H_A$.

For the SMBR unit under consideration, each section is subdivided into two columns of length $L_{\text{col}} = 30$ cm and the total porosity is set to a value of $\epsilon^* = 0.616$, corresponding to a bed void fraction $\epsilon_b = 0.40$, and a particle porosity $\epsilon_p = 0.36$. Considering a switch time of $t^* = 13.33$ min, this SMBR unit is equivalent to the one investigated previously, except for the number of columns in section 3 (Lode et al., 2001).

The differential mass-balance equations for the reacting species within each column are given by

$$\epsilon^* \frac{\partial c_i}{\partial t} + u_j \frac{\partial c_i}{\partial z} = \epsilon_b D_{\text{eff}} \frac{\partial^2 c_i}{\partial z^2} - (1-\epsilon^*) k_m (q_i^{\text{eq}} - q_i) \qquad i = A, E, W \quad (55)$$

$$\frac{\partial q_i}{\partial t} = k_m (q_i^{\text{eq}} - q_i) + \nu_i r_S, \quad (56)$$

with the adsorption equilibria assumed to be linear, that is, $q_i^{\text{eq}} = H_i c_i$, and the reaction taking place in the solid phase only, as described earlier.

All columns are initially devoid of any reacting species, $c_i(0,z) = 0$, and the Danckwerts boundary conditions are assumed to be valid at the inlet and outlet of each column

$$u_j c(z=0^-) = u_j c(z=0^+) - D_{\text{eff}} \left.\frac{\partial c}{\partial z}\right|_{z=0^+} \quad (57)$$

$$\left.\frac{\partial c}{\partial z}\right|_{z=L} = 0.$$

To limit the effect of axial dispersion and mass-transfer resistances on the performance of the unit, an effective dispersion coefficient of $D_{\text{eff}} = 10^{-4}$ cm$^2$/s and a mass-transfer coefficient of $k_m = 10^4\ \text{min}^{-1}$ have been chosen. Under these conditions, the characteristic time for mass transfer is orders of magnitude smaller than the characteristic time for reaction, and the number of theoretical stages per column of the SMBR exceeds a value of 5,000, that is, columns have a very high efficiency.

The behavior of the SMBR as compared to the true moving bed is highlighted here by investigating the dependence of conversion on the flow rate ratios along a line at constant distance from the diagonal in the $(m_2,m_3)$-parameter plane. In particular, these simulations have been performed with $m_3 = 1$, 2, and 3, and $m_2 = m_3 - 0.01$. The results shown in Figure 7 indicate that the conversion decreases from a value of 96.5% at $m_3 = 1.00$ to a value of 70.0% at the highest considered flow rate ratio, that is, $m_3 = 3.00$. While such a decrease in conversion can also be expected for the true countercurrent system, a quantitative comparison reveals a substantial difference in the performances of the two units.

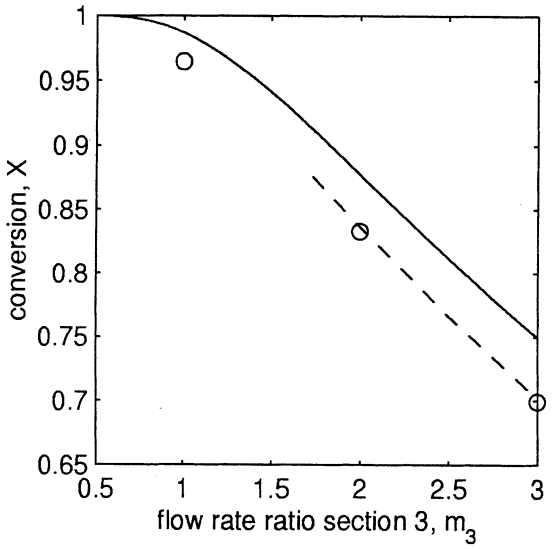


**Figure 7. Effect of flow rate ratios on conversion along a line of constant distance to the diagonal ($m_3 - m_2 = 0.01$).**

Unit configuration 2-2-2-2, switch time $t^* = 13.33$ min. Circles: numerical simulations for detailed SMBR model; solid line: predictions based on TCC model; broken line: predictions based on segregated model.

In particular, by applying the geometric and kinematic conversion rules of Eq. 1, the equivalent Damköhler number for the SMBR unit can be written as

$$Da_3 = \frac{n_3 t^* k_R}{(1-\epsilon_b)}, \quad (58)$$

leading to a value of $Da_3 = 2.60$ for the operating parameters described earlier. The resulting conversion as a function of the flow rate ratio in section 3 is given by Eq. 25, and it is represented in Figure 7 by a solid line, clearly indicating that the conversion obtained in the SMBR is substantially smaller than the one achieved in the TCC unit.

Furthermore, by analyzing the conversion as a function of the flow rate ratio in section 2 for otherwise constant operating parameters, it is found that the amount of reactant converted slightly increases as $m_2$ is reduced (see Figure 8). On the other hand, the conversion in the TCC process is independent of the flow rate ratio in section 2 in the region where $m_3 > m_2 > H_A$.

In order to understand this behavior more clearly, the residence time distribution $E(\tau)$ of an adsorbable reactant within the SMBR unit has to be evaluated. Given the linearity of the system under consideration, the conversion in the unit is entirely determined by the RTD and can therefore be predicted using a reactor model with complete segregation (Fo-

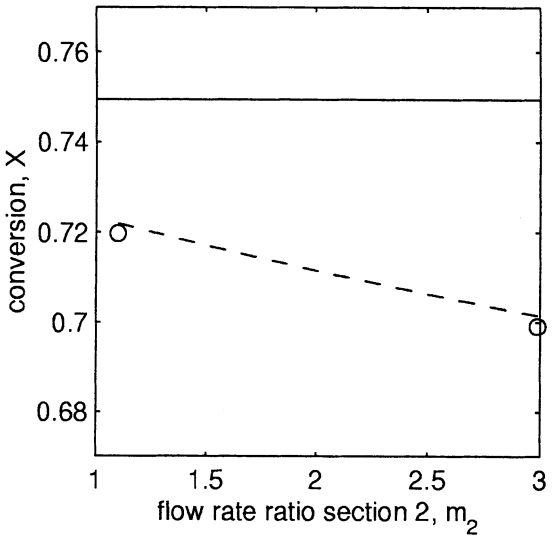


**Figure 8. Effect of flow rate ratios on conversion along a line of constant $m_3 = 3.00$.**

Unit configuration 2-2-2-2, switch time $t^* = 13.33$ min. Circles: numerical simulations for detailed SMBR model; solid line: predictions based on TCC model; broken line: predictions based on the segregation model.

gler, 1997). Accordingly, conversion can be calculated by integrating over all possible residence times the product of the residence time distribution and of the conversion achieved in a batch reactor as a function of residence time

$$X = \int_0^\infty E(\tau) X_{\text{batch}}(\tau)\, d\tau \tag{59}$$

In order to derive the RTD for the SMBR accounting for the presence of the two phases, it is considered that reactant $A$, instead of the classic inert tracer, travels along the SMB reactor under nonreactive conditions. In particular, it is assumed that a constant concentration of $A$ is continuously fed through the feed port to the unit over one switch interval, that is, from $t' = 0$ to $t' = t^*$. The time spent inside the unit before reaching the raffinate outlet is computed for each of these molecules, and the RTD is obtained by properly weighting these internal ages. The standard approach of feeding to the unit just one pulse of species $A$ is not applicable in this case, since the residence time obtained depends upon the injection time of the pulse relative to the switch interval, as will be described below. On the other hand, the behavior of the SMBR during one switch interval is identical to its behavior during the next switch interval, so that sampling one complete switch interval does in fact lead to the correct RTD.

In the following, the RTD is derived for an SMBR with a configuration of two columns in each section and with flow rate ratios in sections 2 and 3 that are larger than the Henry coefficient of $A$, that is, $m_3 > m_2 > H_A$. At these conditions, the propagation velocity of species $A$ within these two sections

$$v_{A,j} = \frac{\left[m_j(1-\epsilon^*)+\epsilon^*\right] L_{\text{col}}}{\left[H_A(1-\epsilon^*)+\epsilon^*\right] t^*}, \quad j = 2, 3 \tag{60}$$

is high enough to allow all molecules fed in a single switch interval to be collected in the raffinate stream and, in addition, to travel for a greater distance than the length of a single column within one complete switch interval, since $v_{A,j} t^* > L_{\text{col}}$.

Among the molecules of species $A$ leaving the unit, several subsets can be distinguished, depending on their "history" within the SMB. First, some molecules travel from the feed node to the raffinate node without experiencing any port switching (first subset), that is, they reach the raffinate before the port switch. The molecules of the second subset are in the second column of section 3 at the end of the switch interval. Therefore, they experience the port switching and actually reach the raffinate in the following switch interval, but they never enter section 2. Finally, the molecules in the third subset are in the first column of section 3 at the end of the switch interval and therefore enter section 2 with the port switch. Distinguishing between these subsets, it is possible to calculate the RTD for any set of $(m_2, m_3)$ values, within the boundaries just indicated. For the case where each molecule can enter section 2 at most once, that is, for the range of operating parameters fulfilling the following constraint

$$\frac{L_{\text{col}}}{v_{A,3}} + \frac{L_{\text{col}}}{v_{A,2}} < t^*, \tag{61}$$

the procedure to obtain the residence time (as well as the definitions of the new symbols introduced in the equations below) is reported in the Appendix, and leads to

$$E(\tau) = \begin{cases} \left(1 - \dfrac{2L_{\text{col}}}{v_{A,3} t^*}\right) \delta\left(\tau - 2\dfrac{L_{\text{col}}}{v_{A,3}}\right) & \text{for } 0 \le \tau < 3\dfrac{L_{\text{col}}}{v_{A,3}} \\ \dfrac{L_{\text{col}}}{v_{A,3} t^*} \delta\left(\tau - 3\dfrac{L_{\text{col}}}{v_{A,3}}\right) + \dfrac{t'_3 - (t^* - L_{\text{col}}/v_{A,3})}{t^*(\tau_{3,1} - 3L_{\text{col}}/v_{A,3})} & \text{for } 3\dfrac{L_{\text{col}}}{v_{A,3}} \le \tau < \tau_{3,1} \\ \dfrac{t^* - t'_3}{t^*(3L_{\text{col}}/v_{A,3} + L_{\text{col}}/v_{A,2} - \tau_{3,2})} & \text{for } \tau_{3,2} \le \tau \le \dfrac{3L_{\text{col}}}{v_{A,3}} + \dfrac{L_{\text{col}}}{v_{A,2}} \\ 0 & \text{for } \tau > \dfrac{3L_{\text{col}}}{v_{A,3}} + \dfrac{L_{\text{col}}}{v_{A,2}}. \end{cases} \tag{62}$$

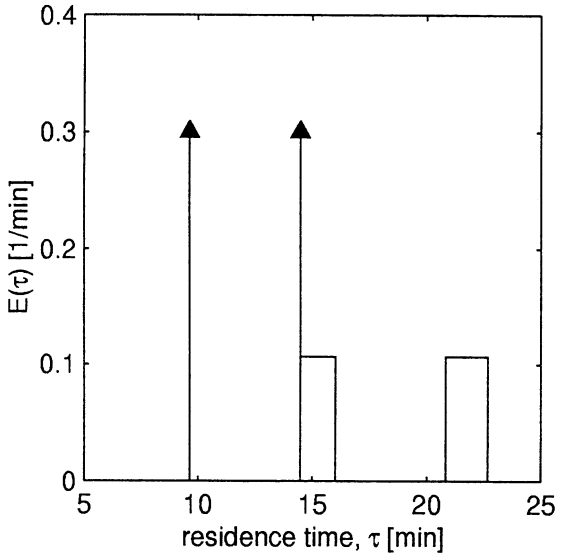


**Figure 9. Residence-time distribution for the case of $m_2 = 1.10$ and $m_3 = 3.00$, switch time 13.33 min.**

Note here that the constraint of Eq. 61 is more restrictive than $m_3 > m_2 > H_A$, which only requires each individual term on the lefthand side of this inequality to be smaller than $t^*$.

For the case of $m_3 = 3.00$ and $m_2 = 1.10$, the corresponding RTD is shown in Figure 9. The two Dirac delta functions originate from tracer molecules that have never entered section 2, and the distance between the two peaks is given by the residence time of reactant $A$ in one single column of section 3. The two rectangular regions at higher residence times, on the other hand, refer to molecules experiencing a smaller fluid velocity within section 2 as compared to the one in section 3.

In order to calculate the conversion in the SMBR unit, the integral in Eq. 59 has to be evaluated. Here, attention has to be paid to the fact that the batch-reactor conversion has to be derived for a heterogeneous system. In particular, the corresponding material-balance equation is given by

$$[\epsilon^* + (1-\epsilon^*)H_A]\frac{dc_A}{d\tau} = -k_R c_A = -\epsilon^* k_L c_A - (1-\epsilon^*)H_A k_S c_A, \quad (63)$$

leading to the following expression for the conversion as a function of time

$$X_{\text{batch}} = 1 - \exp\left(-\frac{k_R \tau}{\epsilon^* + (1-\epsilon^*)H_A}\right) \quad (64)$$

The conversion values computed for the operating points along a line of unitary slope in the $(m_2, m_3)$ plane are shown by the broken line in Figure 7. It is seen that the conversion values computed from the RTD model and through the detailed SMBR model coincide within the region of flow rate ratios considered. The same conclusion is reached when considering the data shown in Figure 8. In particular, the increasing trend in conversion exhibited by the SMBR for decreasing flow rate ratios in section 2 is correctly reproduced, as compared to the constant behavior given by the TCC model. This behavior is due to the increasing residence times in section 2 resulting from lower $m_2$ values, that is, lower fluid velocities.

## Conclusions

To describe the behavior of a true countercurrent reactive chromatography process in terms of reactant conversion and product separation, the concentration profiles inside the unit have been derived analytically using an equilibrium theory model. Based on this solution, expressions for the reactant conversion as a function of the flow rate ratios as well as of the Damköhler numbers within the central sections of the unit have been derived for both an irreversible and a reversible reaction, where $A$ gives $B$ and $C$ and the adsorption equilibria are linear. In the case of an irreversible reaction, explicit design criteria have been derived for the Damköhler numbers, as well as for the flow rate ratios, in order to obtain optimum process performance in terms of productivity and solvent consumption at a constant degree of conversion, that is, for specified product purities.

Although valid only under specific conditions, the solution of the TCC model that has been developed indicated the possibility of using the true countercurrent reactor model as an approximation for the simulated moving-bed reactor. This equivalence between TCC and SMB is widely used for nonreactive, purely separative processes, even when the number of columns is relatively small. However, a clear disagreement between the analytical TCC model results in the presence of reactions, and the ones obtained from the numerical simulation of the SMBR was found for units with a finite number of columns per section. This inequivalence is due to the difference in the residence-time distributions in the two units. This conclusion has been confirmed by comparing the results of the SMBR model given with those obtained by first calculating the residence-time distribution of the SMBR and then applying the model of complete segregation to calculate conversion in the case of linear reaction kinetics. Of course, in the case where the number of columns in the SMBR is very large, the switch time in the SMBR is very small and the RTDs of the SMBR and the TCCR become very similar. However, this is a situation of little interest in practical applications. Therefore, it can be concluded that, contrary to what is commonly done for separative systems, the analogy with the corresponding reactive TCC unit cannot be used when dealing with SMBRs of practical relevance. In these cases, the results obtained through simplified or detailed TCCR models can be used as initial estimates to be refined using a detailed SMBR model.

## Acknowledgments

Financial support of Roche AG, Basel, Switzerland, is gratefully acknowledged.

## Notation

$c_{i,j}$ = liquid-phase concentration of species $i$ within section $j$
$Da_j$ = Damköhler number in section $j$

$D_{\text{eff}}$ = axial dispersion coefficient
DR = desorbent requirement
$E(\tau)$ = residence-time distribution
$H_i$ = Henry coefficient of species $i$
$K_{\text{eq}}$ = reaction equilibrium constant
$k_L$ = liquid-phase reaction rate constant
$k_m$ = mass-transfer coefficient
$k_R$ = overall reaction rate constant
$k_S$ = solid-phase reaction rate constant
$L_{\text{col}}$ = column length
$L_j$ = length of section $j$
$m_j$ = flow rate ratio
$n_j$ = number of columns in section $j$
$n_{sw,j}$ = number of switches experienced by a molecule in section $j$
$P_i^E$ = purity of species $i$ in the extract stream
$P_i^R$ = purity of species $i$ in the raffinate stream
PR = productivity
$q_{i,j}$ = solid-phase concentration of species $i$ within section $j$
$r$ = overall reaction rate per unit volume
$r_L$ = liquid-phase reaction rate
$r_S$ = solid-phase reaction rate
$s$ = parameter along characteristic
$t$ = time
$t'$ = time during switch interval
$t^*$ = switch time
$u_j$ = linear velocity of the liquid phase in section $j$
$u_s$ = linear velocity of the solid phase in section $j$
$v_{i,j}$ = propagation velocity of species $i$ in section $j$
$x_j$ = dimensionless time coordinate
$X$ = conversion
$y_j$ = dimensionless space coordinate
$z$ = space coordinate

### *Greek letters*

$\alpha$ = fraction of molecules
$\beta$ = fraction of molecules
$\beta_j$ = dimensionless quantity, Eq. 47
$\gamma_j$ = dimensionless quantity, Eq. 48
$\delta(\tau)$ = Dirac delta function
$\epsilon^*$ = total porosity
$\epsilon_b$ = bed porosity
$\epsilon_p$ = particle porosity
$\nu_i$ = stoichiometric coefficient of species $i$
$\sigma_{i,j}$ = slope of the characteristic for species $i$ in section $j$
$\tau$ = residence time

### *Subscripts and superscripts*

$i$ = species $i$, $i = A,B,C$
$j$ = section $j$
opt = at optimum operation point
$a$ = state at lefthand boundary outside of a section
$b$ = state at righthand boundary outside of a section
$D$ = desorbent stream
$E$ = extract stream
eq = at equilibrium with the fluid phase
$F$ = feedstream
$I$ = initial state
$R$ = raffinate stream
SMB = simulated moving bed process
TCC = true countercurrent process
0 = state at lefthand boundary inside of a section
1 = state at righthand boundary inside of a section

## Literature Cited


Akintoye, A., G. Ganetsos, and P. E. Barker, "The Inversion of Sucrose on a Semi-Continuous Counter-Current Chromatographic Bioreactor-Separator," *Trans. Inst. Chem. Eng.*, **69**(C), 35 (1991).

Barker, P. E., G. Ganetsos, A. Ajongwen, and A. Akintoye, "Bioreaction-Separation on Continuous Chromatographic Systems," *Chem. Eng. J.*, **50**, B23 (1992).

Duennebier, G., J. Fricke, and K.-U. Klatt, "Optimal Design and Operation of Simulated Moving Bed Chromatographic Reactors," *Ind. Eng. Chem. Res.*, **39**, 2290 (2000).

Fogler, H. S., *Elements of Chemical Reaction Engineering*, Prentice Hall, Upper Saddle River, NJ (1992).

Hashimoto, K., S. Adachi, H. Noujima, and Y. Ueda, "A New Process Combining Adsorption and Enzyme Reaction for Producing Higher-Fructose Syrup," *Biotechnol. Bioeng.*, **25**, 2371 (1983).

Kawase, M., Y. Inoue, T. Araki, and K. Hashimoto, "The Simulated-Moving-Bed Reactor for Production of Bisphenol A," *Catal. Today*, **48**, 199 (1999).

Kawase, M., A. Pilgrim, T. Araki, and K. Hashimoto, "Lactosucrose Production Using a Simulated Moving Bed Reactor," *Chem. Eng. Sci.*, **56**, 453 (2001).

Kawase, M., T. B. Suzuki, K. Inoue, K. Yoshimoto, and K. Hashimoto, "Increased Esterification Conversion by Application of the Simulated Moving Bed Reactor," *Chem. Eng. Sci.*, **51**, 2971 (1996).

Lode, F., M. Houmard, M. Mazzotti, and M. Morbidelli, "Continuous Reactive Chromatography," *Chem. Eng. Sci.*, **56**, 269 (2001).

Mazzotti, M., A. Kruglov, B. Neri, D. Gelosa, and M. Morbidelli, "A Continuous Chromatographic Reactor: SMBR," *Chem. Eng. Sci.*, **51**, 1827 (1996).

Shieh, M. T., and P. E. Barker, "Saccharification of Modified Starch to Maltose in a Semi-Continuous Counter-Current Chromatographic Reactor-Separator (SCCR-S)," *J. Chem. Technol. Biotechnol.*, **63**, 125 (1995).

Shieh, M. T., and P. E. Barker, "Combined Bioreaction and Separation in a Simulated Counter-Current Chromatographic Bioreactor-Separator for the Hydrolysis of Lactose," *J. Chem. Technol. Biotechnol.*, **66**, 265 (1996).

Storti, G., M. Masi, R. Paludetto, M. Morbidelli, and S. Carrá, "Adsorption Separation Processes: Countercurrent and Simulated Countercurrent Operations," *Comput. Chem. Eng.*, **12**, 475 (1988).


## Appendix

To calculate the RTD, an SMB initially devoid of any molecules of $A$ is considered, to which species $A$ is fed only during the first switch interval, $0 \le t' < t^*$. In addition to the condition that will be developed later, this analysis applies to the case where $m_3 > m_2 > H_A$, which guarantees not only that all molecules fed leave the unit through the raffinate stream, but also that in each section component $A$ covers a distance within one switch-time interval that is longer than a single column, that is, $v_{A,j}t^* > L_{\text{col}}$. Among the molecules leaving the unit, three subsets have to be distinguished:

- Molecules of subset 1 do not experience any port switching and leave the unit within the first switch interval, $0 \le t' < t^*$. Their residence time is given by

$$\tau_1 = \frac{2L_{\text{col}}}{v_{A,3}}, \tag{A1}$$

and accordingly, these molecules have to be fed to the unit within the time interval $0 \le t' < t'_1$, with

$$t'_1 = t^* - \tau_1 = t^* - 2L_{\text{col}}/v_{A,3}. \tag{A2}$$

The total fraction of the feedstream experiencing this situation is therefore given by

$$\alpha = \frac{1}{t^*}\left(t^* - \frac{2L_{\text{col}}}{v_{A,3}}\right) = 1 - \frac{2L_{\text{col}}}{v_{A,3}t^*}. \tag{A3}$$

- Molecules of subset 2 experience at least one switching of the ports, but never enter into section 2. For the standard

unit configuration of two columns in each section, this subset is given by all the molecules present in the second column of section 3 at the end of the feed interval, that is, at $t' = t^*$. These molecules have been fed to the unit within the time interval $t'_1 \le t' < t'_2$, with

$$t'_2 = t^* - L_{\mathrm{col}}/v_{A,3}, \tag{A4}$$

and accordingly this subset of molecules accounts for a fraction of

$$\beta = \frac{1}{t^*}(t'_2 - t'_1) = \frac{L_{\mathrm{col}}}{v_{A,3}t^*} \tag{A5}$$

of the total amount of species $A$ fed.

In principle, a fraction of these molecules is eluted to the raffinate within the second switch interval, $t^* \le t' < 2t^*$, while the remaining ones experience one or more additional port switches, depending on the propagation velocity of species $A$ in section 3, $v_{A,3}$, and thus depending on the flow rate ratio in this section. None of these molecules is shifted into section 2.

For the sake of clarity, the analysis is here restricted to the case where all molecules of this subset are eluted during the second switch interval. This requires the molecules to travel at least a distance of two column lengths during one complete switch cycle, and the required propagation velocity is thus lower bounded by

$$v_{A,3} > 2\frac{L_{\mathrm{col}}}{t^*}. \tag{A6}$$

Under these conditions, each of the molecules experiences exactly one switch of the ports, and therefore has to travel a distance of $(2+1)L_{\mathrm{col}}$ before being eluted with the raffinate stream, leading to a residence time of

$$\tau_2 = \frac{3L_{\mathrm{col}}}{v_{A,3}}. \tag{A7}$$

- Finally, subset 3 comprises all the molecules that are present within the first column of section 3 at the end of the feed interval, that is, at $t' = t^*$, and are thus moved into section 2 by the column movement.

Within section 2, these molecules experience a lower propagation velocity than in section 3 due to the lower flow rate ratio, and therefore a calculation of their internal age has to take into account the distance traveled by each molecule in section 2, in addition to that in section 3.

For the sake of clarity, the analysis is restricted here to the case where all molecules entering section 2 due to the column shifting at $t' = t^*$ are either eluted to the raffinate during the second switch interval or can at least proceed to the second column of section 3. This constraint requires a molecule to be able to travel within one switch interval at least a distance of one column length at the propagation velocity in section 2 and an additional one at the corresponding velocity in section 3, thus imposing a lower bound on the propagation velocities, that is

$$\frac{L_{\mathrm{col}}}{v_{A,3}} + \frac{L_{\mathrm{col}}}{v_{A,2}} < t^*. \tag{A8}$$

The set of molecules eluted directly to the raffinate comprises all molecules fed during the interval $t'_2 \le t' < t'_3$, with the critical feeding time $t'_3$ given by

$$t^* = \frac{1}{v_{A,2}}\left[L_{\mathrm{col}} - (t^* - t'_3)v_{A,3}\right] + 2\frac{L_{\mathrm{col}}}{v_{A,3}}. \tag{A9}$$

Each of these molecules has to pass through three columns, with a part of one column being transversed at a reduced velocity. The residence times are therefore uniformly distributed between the one for the molecules being fed at $t' = t'_2$, which are shifted to section 2, but leave the section immediately after the port movement, and the ones being fed at $t' = t'_3$, which are able to elute to the raffinate just prior to the second port shifting. Accordingly

$$\frac{3L_{\mathrm{col}}}{v_{A,3}} \le \tau \le \frac{3L_{\mathrm{col}}}{v_{A,3}} + \left(t^* - \frac{2L_{\mathrm{col}}}{v_{A,3}}\right)\left(1 - \frac{v_{A,2}}{v_{A,3}}\right) = \tau_{3,1}. \tag{A10}$$

The remaining molecules proceed only to the second column of section 3, and hence experience an additional switch of the columns before eluting to the raffinate. The residence times are therefore uniformly distributed between

$$\tau_{3,2} = \frac{4L_{\mathrm{col}}}{v_{A,3}} + \left(t^* - \frac{2L_{\mathrm{col}}}{v_{A,3}}\right)\left(1 - \frac{v_{A,2}}{v_{A,3}}\right) \le \tau \le \frac{3L_{\mathrm{col}}}{v_{A,3}} + \frac{L_{\mathrm{col}}}{v_{A,2}}. \tag{A11}$$

Properly weighting the residence times of these three subsets, the RTD as described by Eq. 62 is obtained.

*Manuscript received Jan. 2, 2002, and revision received Sept. 12, 2002.*